Synthesis, Characterization And Optical Properties Of Samarium Doped Sno$_2$ Nanoparticles

L.P.Chikhale[a], **F.I.Shaikh**[b]

[a] Department of Physics, Venkatesh Mahajan Senior College, Dharashiv (M.S.), India

[b] Department of Forensic Physics, Government Institute of Forensic Science,Chh. Shambhajinagar (M.S.) - 431004, India

Abstract:

In the present investigation, the influence of samarium oxide (Sm_2O_3) on the optical properties were studied. Pristine $SnO_2$and 2.0, 4.0, 6.0 and 8.0 mol% Sm_2O_3 doped samples were prepared using facile co-precipitation route. The samples were characterized by TG-DTA, XRD, FTIR, RAMAN and UV-Vis spectroscopy properties were investigated. The results indicate that Sm_2O_3 inhibits SnO_2 crystal growth. XRD analysis revealed the single phase rutile tetragonal structure of all samples. These results were further confirmed by Raman and FTIR studies. Crystallite size was observed to vary from 17 to 8 nm as the Sm content increased from 0 to 8 mol%, suggesting the prevention of crystal growth with Sm doping. It was evident from the absorption spectra that the absorbance increases with the dopant concentration. Optical band gap was estimated by using Tauc relation which decreases with the increase in Sm content confirming the size reduction as a result of Sm doping. Raman spectroscopic measurements showed thatthe broadening of intense peak observed at 630 cm−1 with Fe doping, indicating that the Sm ions are substituted at the Sn sites in SnO_2 lattice.

Keywords: SnO_2; Sm doping; Screen printing; thick film; XRD.

.

Introduction

Along with hundreds of volatile organic compounds (VOCs) acetone is one of the commonly used chemical reagents in industry, and it easily evaporates at room temperature. People may develop headache, fatigue and even narcosis with the concentration of acetone in air when it exceeds 10,000 ppm. In addition, the medical reports show that along with more than two hundred volatile organic compounds (VOCs), acetone is also a normal constituent of breath of healthy individuals, though in the sub-ppm range, and its concentration increases in diabetic patients. [1,2]. Thus, considering the importance of breath acetone as a biomarker of diabetes, detection and measurement of acetone concentrations in the workplace or human body are necessary for our safety and health. Several analytical techniques have been developed to measure the concentration of acetone, such as gas/liquid chromatographic analysis, spectroscopy and sensors [2–5]. Among them, a sensor isthe most promising method due to their simplicity, precision and convenience. At present, various types of acetone sensors based on semiconductor oxides sensors have been fabricated [2, 6–8]. sensors based on metal oxide semiconductors gain special interest due to their good reproducibility, compact size, ease of use, and low cost [9-11]. SnO_2, as an n-type semiconductor and has been proved to be a highly sensitive material for the detection of both reducing and oxidizing gases [12-15]. Hitherto, extensive studies have been carried out in improving the sensing performance based on the SnO_2 gas sensors, such as adding catalysts, doping metals and metal oxides, decreasing grain size, controlling pore and surface defects[16-18], etc. Among these methods, doping metals or metal oxides on SnO_2 has been proved to be a simple and efficient route to enhance the sensing properties. Many scientific and technological efforts have been made in this field, aiming inimproving the response, selectivity, stability and feasibility for practical use[19-21]. In the present study, we report enhancement in gas sensing properties of pristine and Sm doped nanocrystalline sensors.

2. Experimental

2.1. Preparation of undoped and Sm doped SnO_2 nanopowders

The pristineand Sm:SnO_2 (2 mol%, 4 mol%, 6 mol% and 8 mol%) samples were prepared using facile co-precipitation route. Aldrich make analytical grade reagents were used without further purification. In a typical experiment, an appropriate quantity of stannic chloride ($SnCl_4.5H_2O$) and ammonium hydroxide solution (NH_4OH) were taken. The stannic chloride was dissolved in distilled water to form transparent solution. Dilute ammonia was added drop wise in the above prepared solution under constant magnetic stirring until pH reached around 9-10 where the precipitation of metal cations occurred. The obtained precipitate was filtered, washed several times with distilled water to remove chloride ions [22]. The resulting product was kept for drying under an IR lamp for about 8h, which was followed by calcinations in air at 400°C for 2 h. This sample was labeled as S_0. The Sm:SnO_2 (2 mol%, 4 mol%, 6 mol% and 8 mol%) powder was prepared by using similar way as that of S_0 and the samples were labeled as S_1, S_2, S_3 and S_4 respectively. The Table 1 shows the sample identification of different compositions under investigation.

Sample Code	**Composition**
S_0	Pure SnO_2
S_1	2 mol% Sm_2O_3+98 mole % $SnCl_4$
S_2	4 mol% Sm_2O_3+96 mole % $SnCl_4$
S_3	6 mol% Sm_2O_3+94 mole % $SnCl_4$
S_4	8 mol% Sm_2O_3+92 mole % $SnCl_4$

2.2. Experimental techniques

Thermo-gravimetricand differential thermo-gravimetric analysis (TG–DTA)study of typical sample $S_3$was carried out by using Trans-analytical Instruments SDD2960 in the temperature ranging from room temperature to1000 ^{0}C in the air atmosphere to determine the decomposition temperature and type of reaction. The X-ray diffraction (XRD) patterns of S_0, S_1, S_2, S_3 and S_4were obtained by using BRUKER AXS D8-Advanced X-ray diffractometer using Cu-Kα (λ = 1.5418 Å) radiation. The surface morphology of samplesS_0, S_1, S_2, S_3 and S_4were observed from scanning electron microscopic (SEM) images using JEOL JEM-6700F microscope operating at 5 kV. The elemental composition was obtained by the energy dispersive X-ray spectroscopy (EDAX) technique. FTIR analysis was carried out using a JASCO Model FTIR 6100 type-A spectrometer in the wave number range of 400–4000 cm^{-1} for studying the chemical groups on the surface of samples. The Raman spectra of samplesS_0, S_1, S_2, S_3 and S_4 were taken at room temperature in backscattering geometry, by employing Agiltron Peak Seeker-785 Raman spectrometer with semiconductor laser beam was carried out with the excitation wavelength 785 nm.

3. Results and discussion

3.1. Thermo gravimetric differential temperature studies

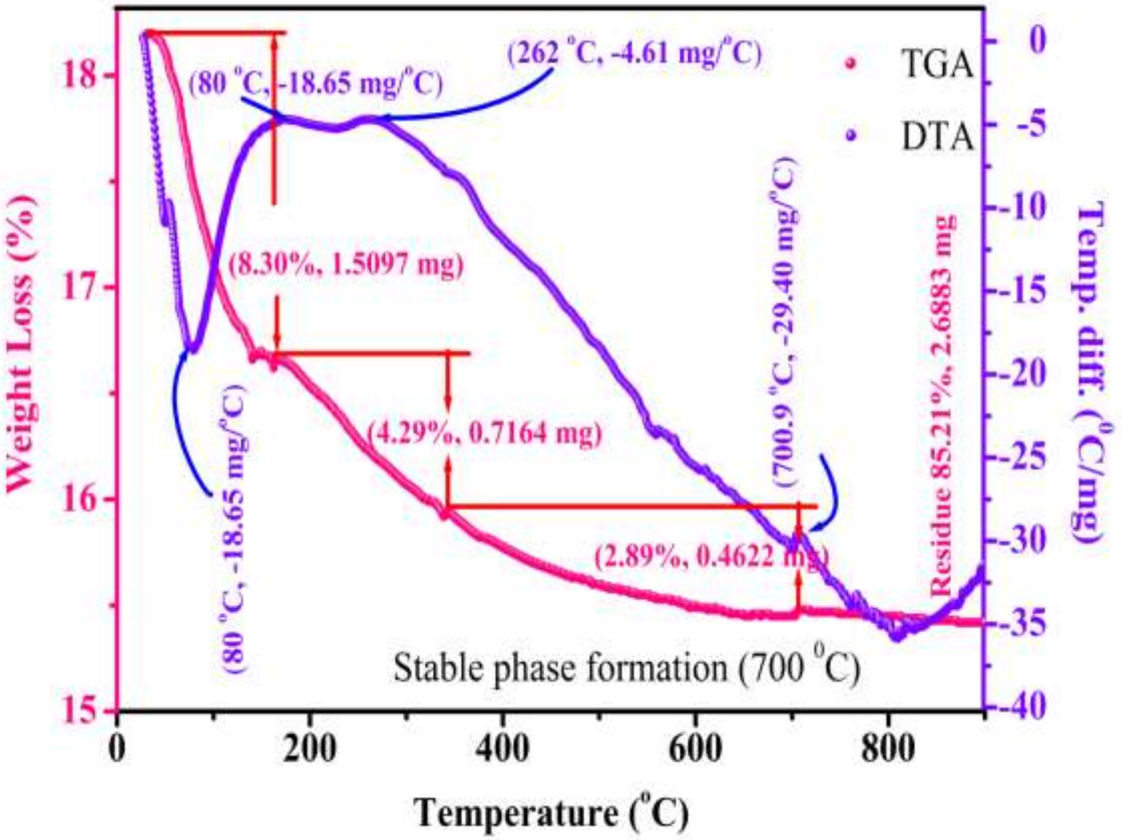

Fig. 1

Fig. 1 shows the TG –DTA curves of the dry precipitated powder of S_3. The TGA curve shows three distinct steps of weight losses; the first step shows a sharp weight loss of ~8.30 % till 164°C. In the second step from 164°C to 339°C we observe 4.29% weight loss. In the third step starting from 339°C we observe a weight loss ~2.89 %.The initial weight loss can be attributed to the desorption of physiosorbed water while the next two regions can be due to the crystallization[26]. The desorption of water appears as an endothermic peak at 80°C.There is no significant weight loss beyond 700ºCindicating complete decomposition of precursors and the phase formation of material.

3.2. X-ray diffraction studies (XRD)

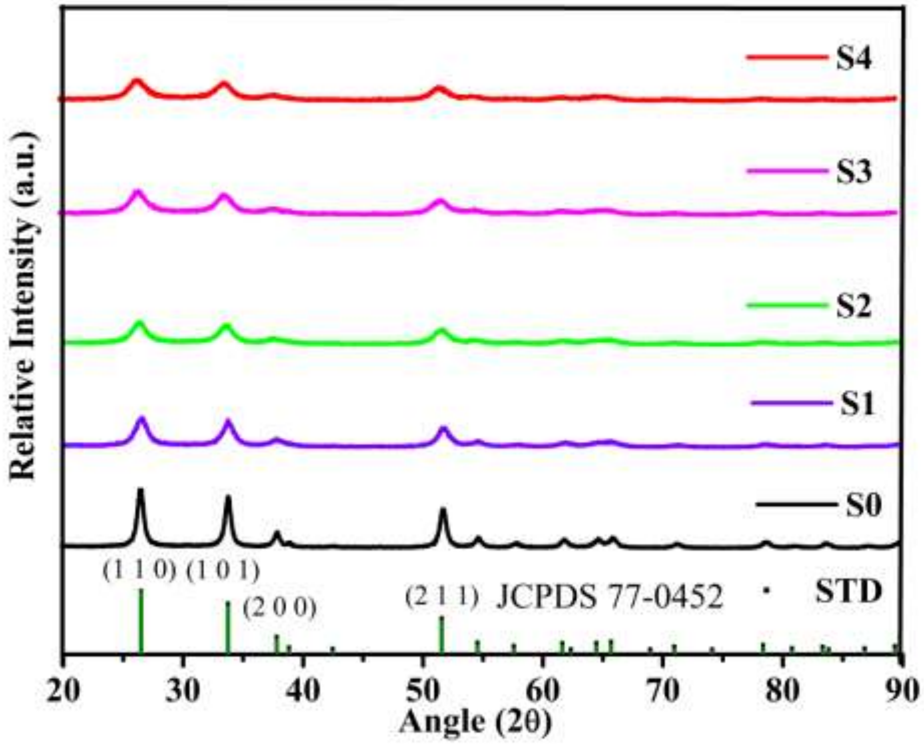

Fig.2

The characteristic XRD patterns of the samplesS_0, S_1, S_2, S_3 and $S_4$are shown in Fig. 2. All the diffraction peaks show tetragonal rutile structure of SnO_2 which are in good agreement with the standard JCPDS card No. 77-0452 with no additional peaks belonging to other phases such as SnO. The prominent peaks correspond to (1 1 0), (1 0 1) and (2 1 1) crystal lattice planes. No peak corresponding to Sm_2O_3 was observed even for 8.0 mol% Sm_2O_3-doped sample; indicating that Sm_2O_3 incorporate into the tin oxide lattice (forming a solid solution), and/or its crystallites are too small to be detected in the XRD. Also, with an increase in Sm_2O_3 content, the relative intensity of the peaks decreases, andthe full width at half-maximum (FWHM) increases. This suggeststhat Sm_2O_3 acts as a crystallite growth inhibitor for SnO_2 material. Other research groups have also shown similar results in the case ofSmdopedSnO_{23}[27, 28] and other rare earth metal oxides [29, 30, 31]. Samarium oxide may prevent the formation of necks and the process of coalescence between particles [27]. The average crystallite size (D) was estimated using the Scherrer equation:

$$D = \frac{0.9\lambda}{\beta\cos\theta}$$

Where, λ, β and θ are the X-ray wavelength, the full width at half maximum (FWHM) of the diffraction peak, and the Braggs diffraction angle, respectively. It is observed that with Sm doping the peaks broaden and relative intensity has reduced, indicating reduction in the crystallite size. The composition with 6.0 mol% $Sm:SnO_2$ shows lowest crystallite size of around 4 nm, clearly indicating size is in the nanometer range. A smaller crystallite size provides a larger surface area for exposure to the test gas, which increases the probability of gas–solid interaction, thereby increasing the response.

Furthermore, the lattice parameters of the samples were calculated from the XRD patterns based on the equation

$$d = \left(\frac{h^2 + k^2}{a^2} + \frac{l^2}{c^2}\right)^{-\frac{1}{2}}$$

Where, (h, k, l) are the indices of crystallographic planes, d the interplanar distance and (a, c) are the lattice parameters. The lattice parameters cell and volume of nano-particles are observed to increase systematically addition of Sm contents. Such a decrease in above parameters can be attributed to the higher ionic radii of Sm^{+3}(64 pm) as compared to Sn^{+4} (71 pm) [32]. These results agree well with the results reported in the literature [33, 34]. Table 2 shows variations in average crystallite size, lattice parameter and cell volume of SnO_2 nanoparticles of different samples.

Sample	**Average crystallite Size (nm) from XRD**	**Lattice Parameter**	
		a (Å)	**c (Å)**
S_0	9.70	4.7141	3.1744
S_1	5.45	4.7282	3.1865
S_2	4.53	4.7387	3.1918
S_3	4.0	4.7458	3.1934
S_4	4.3	4.7492	3.2077

3.3. UV-Vis Studies

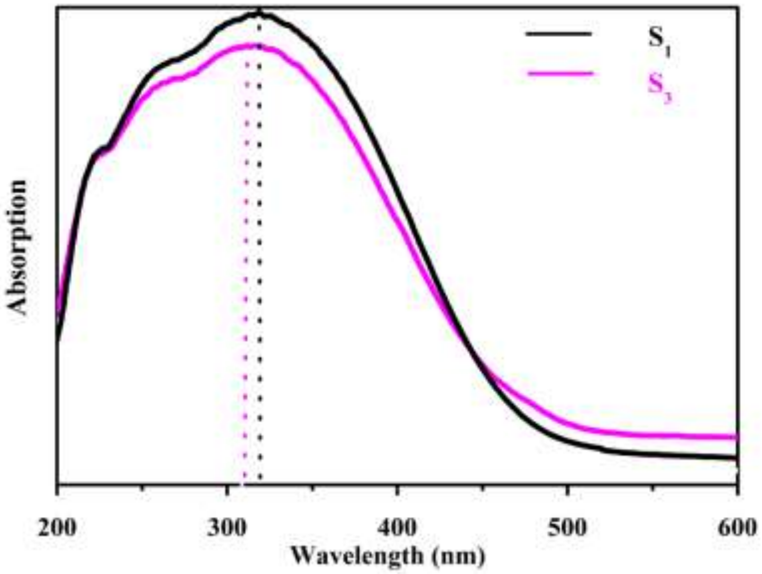

Fig.3

The UV- absorption spectra of prestine and Sm doped SnO_2 were carried out in a JASCO (Model V-670) UV-VIS-NIR spectrophotometer in the wavelength range of 200-1000 nm for studying the band gap energy of the samples S_1, S_2, S_3 and S_4 sintered at 700 ^{0}C. The detailed UV absorption spectra of these samples are shown in Fig.3. It was observed that a strong absorption peak exists around 320 nm for S_0 and around 311 nm for S_3. The corresponding band gap values were 3.87eV and 3.98 eV, respectively. The band gap values were calculated using the relation $Eg = 1240/\lambda$, where λ is the wavelength of the absorption peak in nanometers. The band gap of S_0 matches well with the reported values, while on incorporation of Sm the band gap value increases. In general, majority of metal oxides exhibit only n-type behavior due to the large electronegativity of oxygen with the good conductivity originating from the delocalized conduction band s-like wave function. It results in a significant blue shift of the optical band gap upon doping, which may be true in case of Sm doping observed in the present study.

3.4. FTIR studies

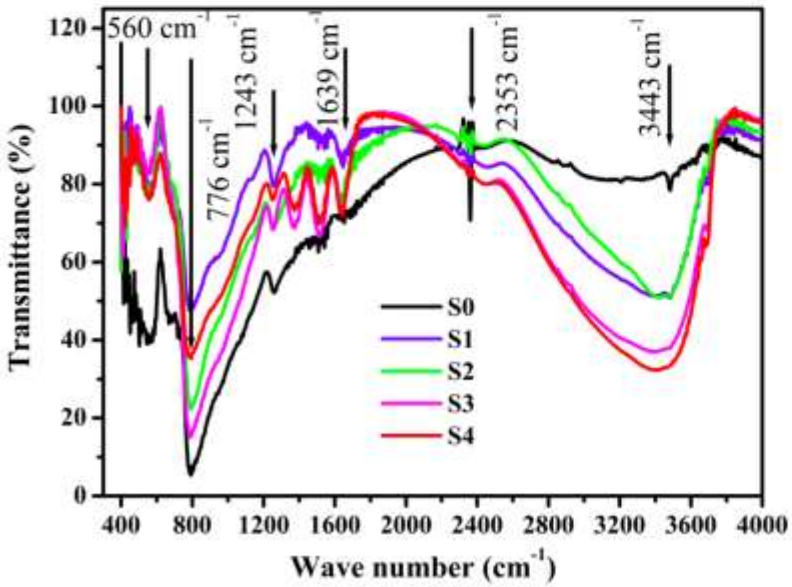

Fig.4

Fig.4 describes FTIR transmittance spectra of S_0, S_1, S_2, S_3 and S_4.The FTIR spectrum is employed to examine presence of chemical groups on the surface of different samples (S_0 to S_4). The broad absorption band between 3225 and 3500 cm^{-1}, the peaks at 1000 and 1230cm^{-1} are attributed to vibration of hydroxyl groups associated with structural water [35]. The bands at 1380and 1600cm^{-1} are assigned to C–H vibrations due to organic trace impurities, incorporated during calcinations process. The bands observed in the range of 450 and 770cm^{-1} are due to the vibration of Sn–O surface cation-oxygen bonds [36]. The typical M–O–M (in this case Sn–O–Sn) vibrations appear in the range of 530–700cm^{-1} [37]. No additional absorption peaks were observed with Sm^{3+}addition, indicating its homogeneous dispersion in the support material.

3.5. Raman spectra studies.

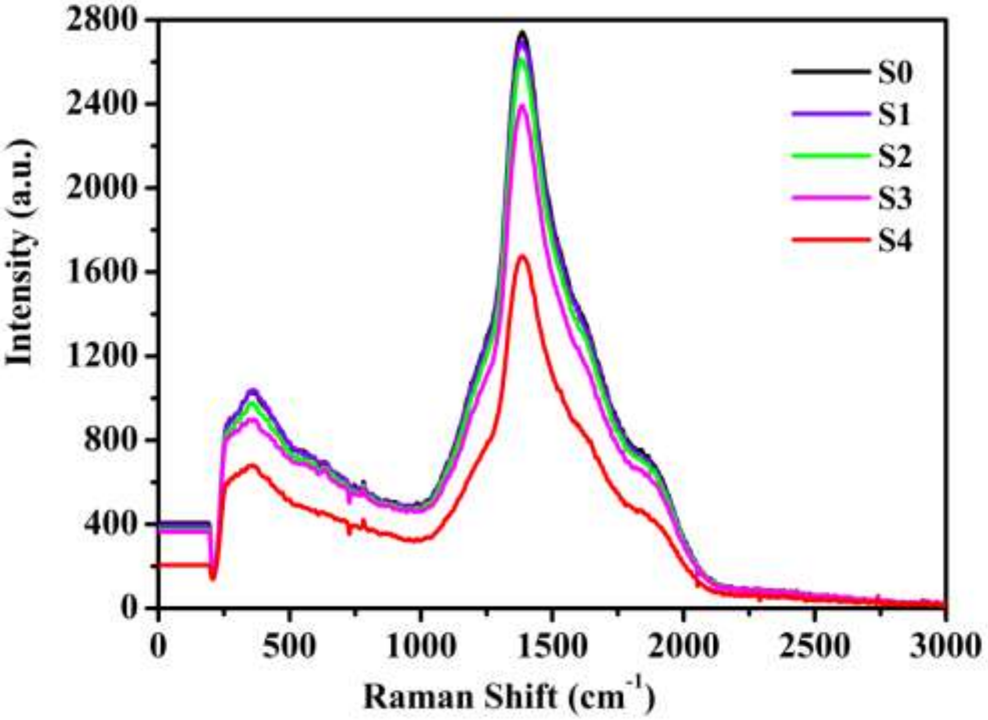

Fig. 5

Fig. 5 shows the Raman spectra of $S_{0,}$ S_1, S_2, S_3 and S_4 samples. All spectra shows two prominent Raman peaks at 476 and 1500 cm^{-1} which are assigned to E_g(translational) and B_{2g} (asymmetric Sn-O stretching) modes of SnO_2 respectively [38]. All these Raman features confirm the tetragonal rutile structure of the SnO_2 sample. The broad peak around 476 cm^{-1} which was reported in extra-fine (3–5 nm) nanoparticles is observed in all the doped samples [39]. This attributes to relaxation of Raman selection rule by reduction in the particle size or by the high concentration of surface defects such as oxygen vacancies and lattice disorder. Another feature to be noted is the decrease in B_{2g} mode intensity in the doped samples [40, 41]. The decrease in the intensity suggests that the dopant interacts strongly with the support and is probably covering the SnO_2 grains with monolayer. The interaction between the Sm^{3+} atoms and the support oxide hinder the crystallization which is reflected in the reduction of peak intensity [42] This is supporting XRD and FTIR results.

4. Conclusions

We have successfully developed nanostructured pristine SnO_2 and (2 mol%, 4 mol%, 6 mol% and 8 mol%) Sm doped SnO_2. The XRD, SEM-EDAX, TEM, SAED, Raman, UV–Vis, FTIR and PL spectroscopic analysis confirmed that the Sm doping in SnO_2 can significantly affects morphology, particle size and band gap of Fe doped SnO_2. These results indicate that the Sm doped SnO_2 material can be used as a potential candidate for fabricating the optoelectronic devices.

References

[1] S.S. Likhodii, K. Musa, S.C. Cunnane, Breath acetone as a measure of systemic ketosis assessed in a rat model of the ketogenic die, Clin. Chem. 48 (2002) 115–120.

[2] N. Makisimovich, V. Vorotyntsev, N. Nikitina, O. Kaskevich, P. Karabun, F. Martynenko, Adsorption semiconductor sensor for diabetic ketoacidosis diagnosis, Sens. Actuator B 36 (1996) 419–421.

[3] C.H. Deng, J. Zhang, X.F. Yu, W. Zhang, X.M. Zhang, Determination of acetone in human breath by gas chromatography–mass spectrometry and solid-phase microextraction with on-fiber derivatization, J. Chromatogr. B 810 (2004) 269–275.

[4] C.H. Deng, W. Zhang, J. Zhang, X.M. Zhang, Rapid determination of acetone in human plasma by gas chromatography–mass spectrometry and solid-phase microextraction with on-fiber derivatization, J. Chromatogr. B 805 (2004) 235–240.

[5] N.D. Totir, S. Velea, C. Lete, C. Neamtu, Pinacol synthesis by acetone reduction coupling, Rev. Chim. 48 (1997) 489–493.

[6] Y. Anno, T. Maekawa, J. Tamaki, Y. Asano, K. Hayashi, Zinc-oxide-based semiconductor sensors for detecting acetone and capronaldehyde in the vapor of consomm'e soup, Sens. Actuators B 24 (1995) 623–627.

[7] S.B. Patil, P.P. Patil, M.A. More, Acetone vapour sensing characteristics of cobalt-doped SnO2 thin films, Sens. Actuators B 125 (2007) 126–130.

[8] Y. Jiang,W. Song, C. Xie, A.Wang, D. Zeng, M. Hu, Electrical conductivity and gas sensitivity to VOCs of V-doped ZnFe2O4 nanoparticles, Mater. Lett. 60 (2006) 1374–1378.

[9] N. Barsan, D. Koziej, U. Weimar, Metal oxide-based gas sensor research: How to? Sens. Actuators B: Chem. 121 (2007) 18–35.

[10] M.S. Wagh, G.H. Jain, D.R. Patil, S.A. Patil, L.A. Patil, Modified zinc oxide thick film resistors as NH3 gas sensor, Sens. Actuators B: Chem. 115 (2006) 128–133.

[11] H.C. Wang, Y. Li, M.J. Yang, Fast response thin film SnO2 gas sensors operating at room temperature, Sens. Actuators B: Chem. 119 (2006) 380–383.

[12] A. Fort, S. Rocchi, M.B. Serrano-Santos, M. Mugnaini, V. Vignoli, A. Atrei, R. Spinicci, COsensing with SnO2-based thick film sensors: surface statemodel for conductance responses during thermal-modulation, Sens. Actuators B: Chem. 116 (2006) 43–48.

[13] K.W. Kim, P.S. Cho, S.J. Kim, J.H. Lee, C.Y. Kang, J.S. Kim, S.J. Yoon, The selective
detection of C2H5OH using SnO2–ZnO thin film gas sensors prepared by combinatorial solution deposition, Sens. Actuators B: Chem. 123 (2007) 318–324.

[14] A.S. Ryzhikov, A.N. Shatokhin, F.N. Putilin, M.N. Rumyantseva, A.M. Gaskov, M. Labeau, Hydrogen sensitivity of SnO2 thin films doped with Pt by laser ablation, Sens. Actuators B: Chem. 107 (2005) 387–391.

[15] J. Yoo, E.D. Wachsman, NO2/NO response of Cr2O3- and SnO2-based potentiometric sensors and temperature-programmed reaction evaluation of the sensor elements, Sens. Actuators B: Chem. 123 (2007) 915–921.

[16] J. Arbiol, J.R. Morante, P. Bouvier, T. Pagnier, E.A. Makeeva, M.N. Rumyantseva, A.M. Gaskov, SnO2/MoO3-nanostructure and alcohol detection, Sens. Actuators B: Chem. 118 (2006) 156–162.

[17] F. Liu, B. Quan, L. Chen, L. Yu, Z. Liu, Investigation on SnO2 nanopowders stored for different time and BaTiO3 modification, Mater. Chem. Phys. 87 (2004) 297–300.

[18] N.S. Ramgir, Y.K. Hwang, S.H. Jhung, I.S. Mulla, J.S. Chang, Effect of Pt concentration
on the physicochemical properties and CO sensing activity of mesostructured SnO2, Sens. Actuators B: Chem. 114 (2006) 275–282.

[19] C.M. Carney, S. Yoo, S.A. Akbar, TiO2–SnO2 nanostructures and their H2 sensing behavior, Sens. Actuators B: Chem. 108 (2005) 29–33.

[20] M. Kugishima, K. Shimanoe, N. Yamazoe, C2H4O sensing properties for thick film sensor using La2O3-modified SnO2, Sens. Actuators B: Chem. 118 (2006) 171–176.

[21] I.T. Weber, A. Valentini, L.F.D. Probst, E. Longo, E.R. Leite, Influence of noble metals on the structural and catalytic properties of Ce-doped SnO2 systems, Sens. Actuators B: Chem. 97 (2004) 31–38.

[22] M. V. Vaishampayan, R. G. Deshmukh, I.S. Mulla, Sens.Actuators B 131 (2008) 665-672.

[23] L. K. Bagal, J. Y. Patil, K. N. Bagal, I. S. Mulla,S. S. Suryavanshi, Mater. Res. Innov.17 (2013) 98-105.

[24] G.H. Jain, L.A. Patil, M.S. Wagh, D.R. Patil, S.A. Patil, D.P. Amalnerkar, Sens. Actuators B 117 (2006) 159-165.

[25] R.C. Pawar, J.S. Shaikh, A.V. Moholkar, S.M. Pawar, J.H. Kim, J.Y. Patil, S.S. Suryavanshi, P.S. Patil, Sens. Actuators B151 (2010) 212-218.

[26] P. Siciliano, Sens.Actuators B 70 (2000)153–164.

[27] S. Habibzadeh, A.A. Khodadadi, Y. Mortazavi, CO and ethanol dual selective sensorof Sm2O3-doped SnO2 nanoparticles synthesized by microwave-inducedcombustion, Sensors and Actuators B 144 (2010) 131–138.

[28] Q. Qi, T. Zhang, X. Zheng, H. Fan, L. Liu, R. Wang, Y. Zeng, Electrical response of Sm2O3-doped SnO2 to C2H2 and effect of humidity interference, Sensors and Actuators B 134 (2008) 36–42.

[29] F. Pourfayaz, A.A. Khodadadi, Y. Mortazavi, S.S. Mohajerzadeh, CeO2 doped SnO2 sensor selective to ethanol in presence of CO, LPG and CH4, Sensors and Actuators B 108 (2005) 172–176.

[30] Z. Jiang, Z. Guo, B. Sun, Y. Jia, M. Li, J. Liu, Highly sensitive and selective butanone sensors based on cerium-doped SnO2 thin films, Sensors and Actuators B 145(2010) 667–673.

[31] C.M. Wang, J.F. Wang, H.C. Chen, W.B. Su, G.Z. Zang, P. Qi, B.Q. Ming, Effectsof Pr2O3 on the nonlinear electrical characteristics and dielectric properties of$SnO_2 \bullet Co_2O_3 \bullet Ta_2O_5$varistor systems, Solid State Communications 132 (2004)163–167.

[32]W.Zenga, T.Liua, D.Liua, E. Hana, Sens.Actuators B 160 (2011) 455-462.

[33]D. Haridas, V. Gupta, Sens. Actuators B167 (2012) 156-164.

[34]T.Rui-qin, G.Yan-qun, Z.Jun-hua, L.Yue, X.Tie, Trans.Nonferrous.met.Soc.China.21(2011) 1568-1573.

[35] D. Chen, L.Gao, J. Colloid Inter. Sci. 279 (2004) 137-142.

[36] R. Adnan, N. A.Razana, I.A.Rahman and M. A.Farrukh, J.Chinese Chem. Soci. 57(2010) 222-229.

[37] L. Jiang, G. Sun, Z. Zhou, S. Sun, Q. Wang, S.Yan,H. Li, J. Tian, J. Guo, B. Zhou, Q.Xin, J. Phys. Chem. B 109 (2005) 8774-8778.

[38]S.K.Pillai,L.M.Sikhwivhilua, T.K. Hillie, Mater. Chem. Phys. 120 (2009) 619-624.

[39] Z. Jianga, Z.Guoa, B. Suna, Y.Jia, M. Li, J.Liua, Sens. Actuators B 145 (2010) 667-673. [40] A. Azama, A. S. Ahmed, S. S. Habib, A.H. Naqvi, J. Alloys Compd.523 (2012) 83-87.

[41] L.L. Xing, B. He, Z.H. Chen, X.Y. Xue, Solid State Sciences 15 (2013) 42-46.

[42] T. N.Soitah, C.Yang ,L.Sun , Mat. Sci.Semicon. Proc. 13 (2010) 125-131.